

Fingering of dense nonaqueous phase liquids in porous media

2. Analysis and classification

Rudolf J. Held and Tissa H. Illangasekare

Department of Civil, Environmental, and Architectural Engineering, University of Colorado, Boulder

Abstract. Fingering of dense nonaqueous phase liquids (DNAPLs) as seen in three-dimensional experiments with saturated, homogeneous porous media was analyzed. A consistent geometrical quantification of finger configurations was obtained using concepts of fractal and multifractal scaling. Fractal patterns that determine the probabilistic distribution of the DNAPL were found to be representative for every experimental combination of sand and DNAPL. These patterns could be attributed to either capillary or viscous fingering regimes. With multifractal formalisms we were able to give a description of the underlying process kinetics. The generalized dimension D_q relates results to diffusion-limited aggregation (DLA) or invasion percolation type models. The spectrum of singularities $f(\alpha)$ is invariable for cross sections of an experiment and in turn can be used for a classification of the displacement system. The width of the $f(\alpha)$ curve in the range of positive moments quantifies displacement instability. Phase transitions are indicated for the more stable displacement systems.

1. Introduction

We presented dense nonaqueous phase liquid (DNAPL) experiments with three-dimensional, saturated porous media in the companion paper [Held and Illangasekare, this issue]. Fingering of DNAPLs is expected to be dissimilar to the fluid displacement studies in petroleum engineering or soil physics. In the latter cases the displacing fluid (water) is preferentially wetting with respect to the medium. Macroscopically conceivable effects, for example, capillary imbibition, can be seen. DNAPL infiltration in a water-saturated medium, by comparison, is the displacement by a nonwetting fluid and should be mainly regarded as a pore-scale process.

Immiscible two-phase flow in porous media was first examined for the recovery of petroleum by water injection into the reservoir formation. Instabilities of the macroscopic interface between water and higher viscous oil brought about extensive work on the phenomenon of viscous fingering (reviewed by Wooding and Morel-Seytoux [1976] and Homay [1987]). For propagation of DNAPLs the inverse process of the organic phase displacing water needs to be investigated.

Soil scientists have focused on wetting front instabilities of water displacing air in the unsaturated zone of an aquifer (reviewed by Gee *et al.* [1991]). For DNAPL infiltration in the unsaturated zone a multiphase system exists with DNAPL, water, and air. Different effects due to relative wettabilities would have to be considered. Displacement by DNAPL above the water table is unconditionally stable from the theoretical viewpoint, and in this case the vaporization of most DNAPLs constitutes a less threatening contamination scenario.

Several factors that generally influence the stability of immiscible displacement and can be related to the problem of DNAPL migration have been stated in the literature [see Peters and Flock, 1981]: (1) fluid viscosity or mobility, (2) gravity, (3) capillary forces, (4) porous media pore structure, permeability,

and wettability, (5) displacement velocity, and (6) system geometry and dimensions. The displacement history (hysteresis), the large-scale flow field, and heterogeneity of porous media properties at various scales are of additional importance in natural systems. Dimensionless parameters such as the Darcy-Rayleigh number, the capillary number, and the viscosity contrast, have been recognized as relevant for displacement instability. The first number relates gravitational to viscous forces, the second relates viscous to interfacial forces, and the last group relates viscosities of the fluids to each other.

Lenormand [1985] proposed a phase diagram for a distinction of different fingering regimes. Three types of interface morphologies were found in experiments, depending on the viscosity ratio M and the capillary number C . These dimensionless parameters were defined as

$$M = \mu_2/\mu_1 \quad (1)$$

$$C = v\mu_2/(A\sigma \cos \theta) \quad (2)$$

where the subscript 2 designates the displacing fluid and the subscript 1 the displaced fluid. The variable θ is the fluid-solid contact angle, σ is the interfacial tension, and A is the cross-sectional area of the sample; hence v/A represents an average interstitial velocity. Figure 1 shows the phase diagram, with regions corresponding to a stable displacement regime, a viscous fingering regime, and a capillary fingering regime. Gravitational and inertial forces were neglected in the two-dimensional study of Lenormand [1985]. A third axis, relating to the influence of gravity, could be thought of as a supplement to this presentation.

To give an idea where our DNAPL experiments would be located in a diagram of the M/C plane, we plotted them onto Figure 1. The viscosity ratio is determined by the two fluids used in an experiment. The capillary number is an estimate, since our three-dimensional setup did not allow the direct determination of displacement velocities. A capillary number was taken as calculated at the spill point, with the cross-sectional area of the spill device known and the average flux

Copyright 1995 by the American Geophysical Union.

Paper number 95WR00429.
0043-1397/95/95WR-00429\$05.00

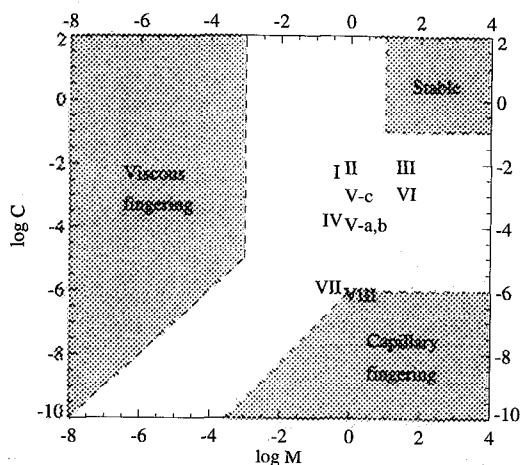


Figure 1. Phase diagram of displacement regimes [after Lenormand, 1985]. Our experiments [cf. Held and Illangasekare, this issue, Table 1] are plotted at the corresponding positions.

recorded during the spill. We deduced that the capillary number did increase during the progress of most experiments, when fingers were created and the flow occurred within a smaller area. Thus the location of our experiments as plotted on the M/C plane may vary with C . Except for VII and VIII, all experiments fall in the transitional zone between distinct fingering regimes as defined by Lenormand [1985].

Besides the qualitative description of experimental observa-

tions [Held and Illangasekare, this issue], a suitable quantification of results is required for the discussion of DNAPL fingering. A quantitative analysis can provide a data set useful for the comparison of experiments or for the validation of theoretical and numerical models. An outcome of our experiments was a great complexity of observed finger patterns. The measurement of finger diameters, finger areas, and finger spacing did not seem adequate for the description of the variety of patterns we encountered. A typical example is shown in Figure 2.

A number of concurrent studies on the use of fractal methods in nonlinear dynamics of fluid displacement in porous media have been reported [e.g., Chandler *et al.*, 1982; Wilkinson and Willemsen, 1983; Paterson, 1984]. Models developed for stochastic aggregation and growth have helped in understanding and in interpreting the formation of fractal structures, that is, growth kinetics are found to be inherently connected to the resulting fractal geometry.

Fractal analysis was employed to describe displacement patterns in Hele-Shaw cells [e.g., Nittmann *et al.*, 1985; Daccord *et al.*, 1986] and also in two-dimensional porous media [e.g., Måløy *et al.*, 1985, 1987; Oxaal *et al.*, 1987]. Clément *et al.* [1985] have examined fractal dimensions obtained in three-dimensional experiments for liquid metal displacing air.

A multifractal analysis was employed by Nittmann *et al.* [1987] and Måløy *et al.* [1987] on viscous fingering structures observed in Hele-Shaw cells and in a monolayer of glass beads, respectively. Recent literature suggests that the multifractal formalism is applicable to three-dimensional systems. The term "multifractal" comes from Frisch and Parisi [1985] and

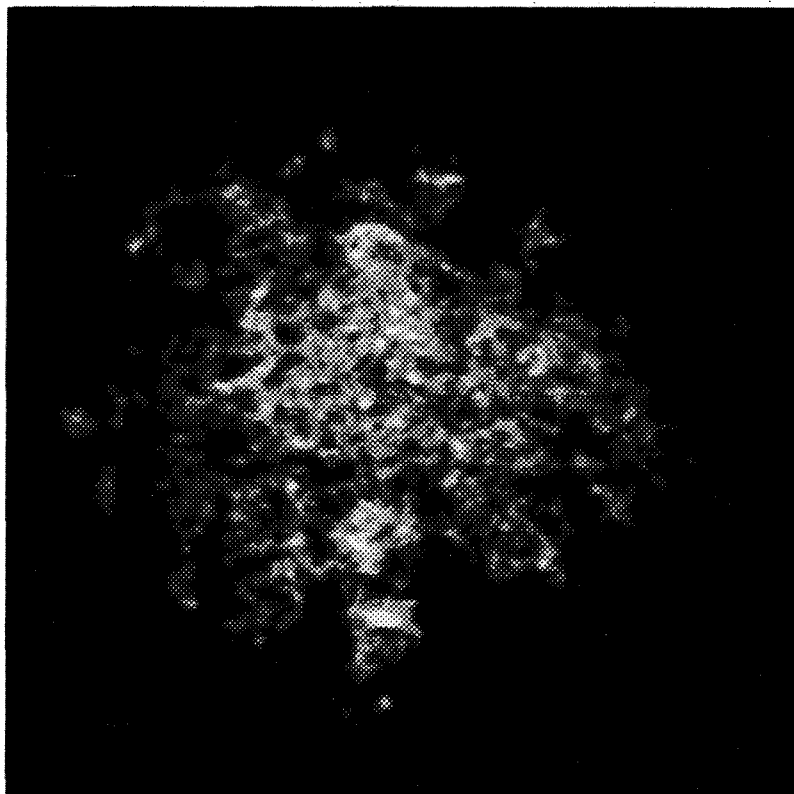


Figure 2. Cross section obtained from experiment VIII (1,1,1-trichloroethane (TCA) and mesh 70 sand) at a sampling depth of 5 cm below the spill point. The image represents an area of 26×26 cm and was processed for better visual contrast between dense nonaqueous phase liquid (DNAPL) (white-gray) and background (set to black).

among several interpretations simply denotes a probabilistic concept or tool [after Mandelbrot, 1989]. A synopsis of analysis and research on fingering phenomena is provided by Feder [1988] or Yortsos [1990].

2. Methods and Theory

Image analysis software was used for further data processing of sections of the DNAPL plumes on digitized records. The recorded working images show a resolution of about 360×360 image elements. Each image element has a gray value assigned from 0 to 255, corresponding to a range from black to white. A low-pass filter with a 3×3 convolution kernel was applied to the recorded images; low-pass filters are commonly employed to contrast real objects from noise in the recorded images.

One way of presenting the information contained in an image is by plotting its intensity histogram, the distribution or frequency of gray levels. For example, the intensity histogram for Figure 2 is given in Figure 3.

The images were analyzed initially by measuring geometric parameters of individual objects. The image analysis system has therefore to discern object boundaries and distinguish object areas from background. An automated separation of objects can be problematic, and even separation of objects by visual inspection is impossible at times (reported by Glass *et al.* [1990] from a study of three-dimensional experiments on fingering). The measurements from statistical object analysis were only meaningful for some of our experiments.

Fractal dimensions offer a systematic approach to quantifying irregular patterns, if they contain a repeated internal structure over a range of scales [Meakin, 1991]. Classical mathematical fractals, such as constructions of the Koch curve or the Sierpiński gasket, are hierarchically generated structures. They are nonrandom, and when scale invariance holds for all scales, the overall distribution is said to be exactly self-similar. Like most fractals in nature, our structures are considered random fractals and only statistically self-similar with a change in scale. This means that the probability distribution describing the geometry, rather than the geometry itself, is self-similar.

The Hausdorff-Besicovitch dimension D is strictly based on a mathematical formalism. One can think of covering a set of points S with shells that are not necessarily of the same size, but have a diameter less than ε [Feder, 1988]. It is very difficult to evaluate D for applications involving arbitrary or real data sets. Alternatively, the box-counting dimension D_b is easier determined. D_b and D are equal for a large class of sets; in general, $D_b \geq D$, since the number of possible covers is reduced by the restriction to only one shell size.

For box counting, a set S is overlaid with a box grid of cell width ε , and the number of boxes $N(\varepsilon)$ that is needed to cover the object is determined. The box-counting dimension D_b is found through the scaling relation of a power law [Mandelbrot, 1982]:

$$N(\varepsilon) \sim \varepsilon^{-D_b} \quad (3)$$

Let $N(\varepsilon)$ be the smallest number of boxes containing an element of the set S ; then

$$D_b(S) = -\lim_{\varepsilon \rightarrow 0} \frac{\log N(\varepsilon)}{\log \varepsilon} \quad (4)$$

provided the limit exists. The infimum of $N(\varepsilon)$ is approximated by varying the origin of the grid until the smallest num-

ber is found. From (4) the box-counting dimension D_b can be determined as the negative slope of $\log N(\varepsilon)$ versus $\log \varepsilon$, measured over a range of box widths. Box counting was done for grid sizes of $\varepsilon = 2^n$ ($n = 1, \dots, 6$), where we could prove a straight-line fit in our initial investigations. In estimating the fractal dimension, a higher weight was assigned to the number of boxes $N(\varepsilon)$ obtained from finer grids. We disregarded boxes of size 1×1 ($n = 0$) on account of the applied low-pass filter.

For a multifractal analysis we treat our data as a measure; therefore we incorporate the gray level information of our images. In terms of box counting, a probability or weight is given for the contents of each box (here the DNAPL saturation obtained by integrating gray levels). The notion of the coarse Hölder exponent α is adapted with

$$\alpha = \frac{\log \mu(\text{box})}{\log \varepsilon} \quad (5)$$

that is, the logarithm of the integrated measure of the box μ normalized by the size of the box. Here, α represents the singularity strength of μ , i.e., how μ grows with ε . A frequency distribution of α can be obtained by evaluating the number $N_\varepsilon(\alpha)$ of boxes of size ε in analogy with (3) and (4). When $\varepsilon \rightarrow 0$, such a function of α converges under certain conditions to the limiting function $f(\alpha)$. The values of $f(\alpha)$ may be loosely interpreted as fractal dimensions [Feder, 1988], conceptually, Hausdorff-Besicovitch dimensions for subsets of the measure having the same coarse Hölder exponent α .

There are several methods to examine the multifractal behavior of experimental data. The analytical scaling relations we used are based on the method of moments [after Halsey *et al.*, 1986] and were implemented with a box-counting algorithm. The method of moments is applicable to a restricted class of multifractal measures, yet was considered appropriate in our investigation (see below).

In theory, a partition function is defined as

$$\chi_q(\varepsilon) = \sum_{i=1}^{N(\varepsilon)} \mu_i^q \quad (6)$$

where q is any real number. Divided by the total number of boxes, $\chi_q(\varepsilon)$ yields the normalized q th moment of the sample. Scaling for $\chi_q(\varepsilon)$ takes the form $\chi_q(\varepsilon) \sim \varepsilon^{\tau(q)}$ or

$$\tau(q) = \lim_{\varepsilon \rightarrow 0} \frac{\log \chi_q(\varepsilon)}{\log \varepsilon} \quad (7)$$

Hence the function $\tau(q)$ describes the distribution of moments in the measure. As $q \rightarrow \infty$ the largest μ_i , equivalent to the densest parts of the measure, dominate the sum in (6). Conversely, as $q \rightarrow -\infty$ the smallest μ_i or the least concentrated parts are accentuated [Jensen, 1987].

When both $\tau(q)$ and $f(\alpha)$ are differentiable functions, they can be linked to one another by Legendre transformation. The set of variables τ and q is transformed to the variables f and α , and vice versa, by

$$\alpha(q) = \frac{\partial}{\partial q} \tau(q) \quad (8)$$

$$f(\alpha(q)) = q\alpha(q) - \tau(q) \quad (9)$$

Here, $f(\alpha)$ curves are often obtained analytically from $\tau(q)$ with Legendre transformation. A direct determination of $f(\alpha)$

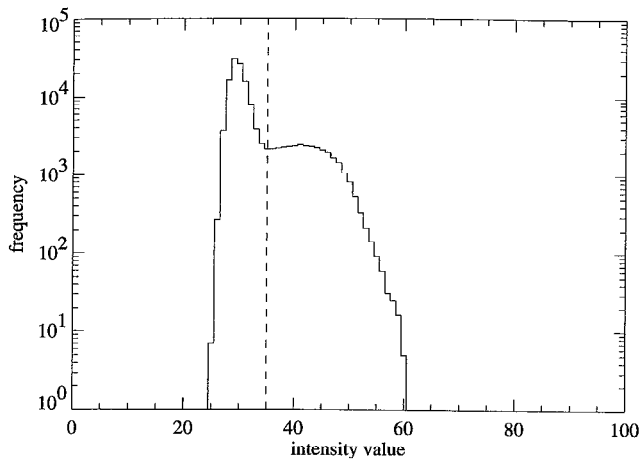


Figure 3. Intensity histogram for Figure 2.

was proposed by *Chhabra and Jensen* [1989] that is well suited to analyze limited experimental data. Their method produces especially accurate results in the sampling region around $q = 0$. The algorithm of *Chhabra and Jensen* [1989] builds on the same computational steps as the method of moments with box counting and was given preference in this work.

Another notion was introduced by *Hentschel and Procaccia* [1983] with the generalized dimension D_q , where D_q is simply derived from $\tau(q)$ by $\tau(q) = (q - 1)D_q$. This provides an alternative description of multifractal measures. Referring to (4) and (7), it can be seen that D_q at $q = 0$ equals D_b , the box-counting dimension. The singularity in the definition of D_q at $q = 1$ was evaluated after *Feder* [1988].

The practical computation of $\tau(q)$, D_q , and $f(\alpha)$ required including all gray levels of the recorded image. Our decision to work with the image as a whole is addressed in the next sections. The smallest intensity value of an image was shifted to the origin for a normalization of the measure. This results in no loss of generality. Multifractal analysis was pursued by coarse graining the measure with boxes of size $\varepsilon = 2^n$ ($n = 1, \dots, 6$) and the determination of the corresponding box measure μ_i . The partition function was computed from (6) for all values of ε and for q varied from -10 to $+10$.

3. Results

A gray level range from 24 to 61 can be taken as characteristic for most of the images. The peak in the histogram distribution of Figure 3 corresponds to background readings, whereas the right part of the histogram reflects the DNAPL distribution. A clear distinction of background and DNAPL ranges is not seen in the histogram. By optical interpretation of the image the gray level that separates background and chemical information falls on a value of 35.

Statistical analysis in the sense of measuring finger areas, diameter, and spacing was applicable to certain experiments. For experiments in coarse sand the mean areas were measured as $0.24 \pm 0.4 \text{ cm}^2$ (experiment I with trichloroethylene (TCE)) and $0.28 \pm 0.4 \text{ cm}^2$ (experiment II with 1,1,1-trichloroethane (TCA)). The large error margins indicate just the high variability of the measurements. In experiment IV with medium sand and TCE the average finger areas were $0.44 \pm 0.7 \text{ cm}^2$; they can also be given as $8.6 \pm 1.9 \text{ cm}^2$ and $8.5 \pm 1.9 \text{ cm}^2$ for experiment V-a and experiment V-b (medium sand and TCA).

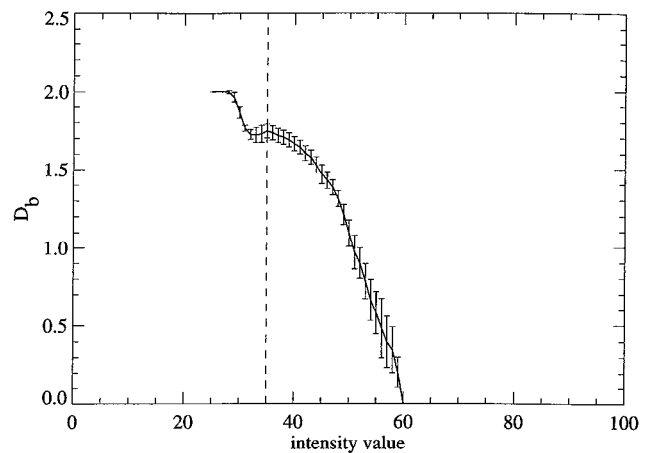


Figure 4. Box-counting dimensions calculated for Figure 2 with varied intensity threshold values.

In all other cases a statistical object analysis did not represent measurements on isolated fingers.

3.1. Fractal Analysis

In this section we present results as they are attained from data sets; the selection of a gray level threshold implies a binary discrimination of the data. With a threshold level of 35 for Figure 2, i.e., eliminating the background information in the picture, we performed box counting on the perimeter and on the entire set. A power law in scaling of the perimeter was lacking, especially at high resolutions. An indication of fractality of the entire set was given over about 2 orders of magnitude in length scale, from millimeters to tens of centimeters.

For the comprehensive investigation of an image the threshold was shifted over the range of existing gray levels, and box-counting dimensions for the entire set were determined. The error margins of this determination increased with higher thresholds as the size of the set was reduced. A deviation from strict power law behavior was then observed at large scales. Figure 4 shows the resulting D_b for the above example. At the lowest threshold of 24 the picture is completely filled ($D_b = 2.0$). The fractal dimension initially degrades, when the threshold value is augmented, until D_b shows an intermediate maximum at a gray level of 35. This response in the curve is attributed to the fractal nature of the DNAPL distribution. It is suggested that the highest fractal dimension would be at the gray level where the DNAPL first appears in an image. However, background readings overlap in that gray level range. The maximum in D_b did correspond to the threshold between DNAPL and background found from visual inspection.

An intermediate maximum in the box-counting dimensions was identified in every image. The function of D_b versus gray level beyond this point reproduced the features of the intensity histogram (compare with Figure 3). Convexity or concavity in the shape of the histogram curve was strictly preserved in the spectrum of D_b .

A plot was developed which combines the box-counting dimensions of all horizontal cross sections from one experiment. Each spectrum was normalized by removing the part to the left-hand side of the intermediate maximum (shifting the spectrum from gray level 35 to zero in Figure 4). An overview of several parameters, i.e., penetration depth, relative intensity variation, and fractal dimensions, is intended. The overall pat-

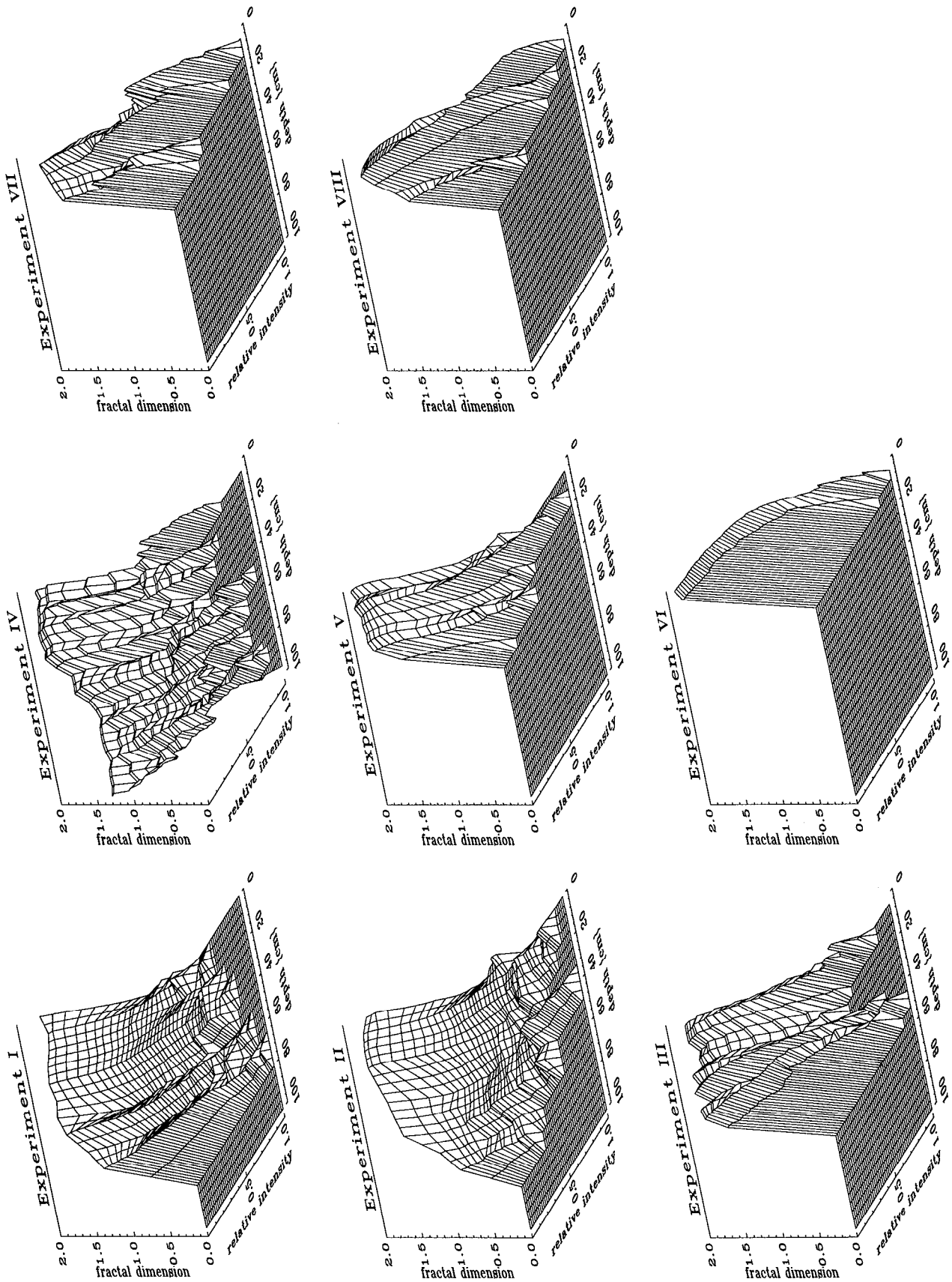


Figure 5. Fractal patterns for DNAPL experiments (see text for explanation).

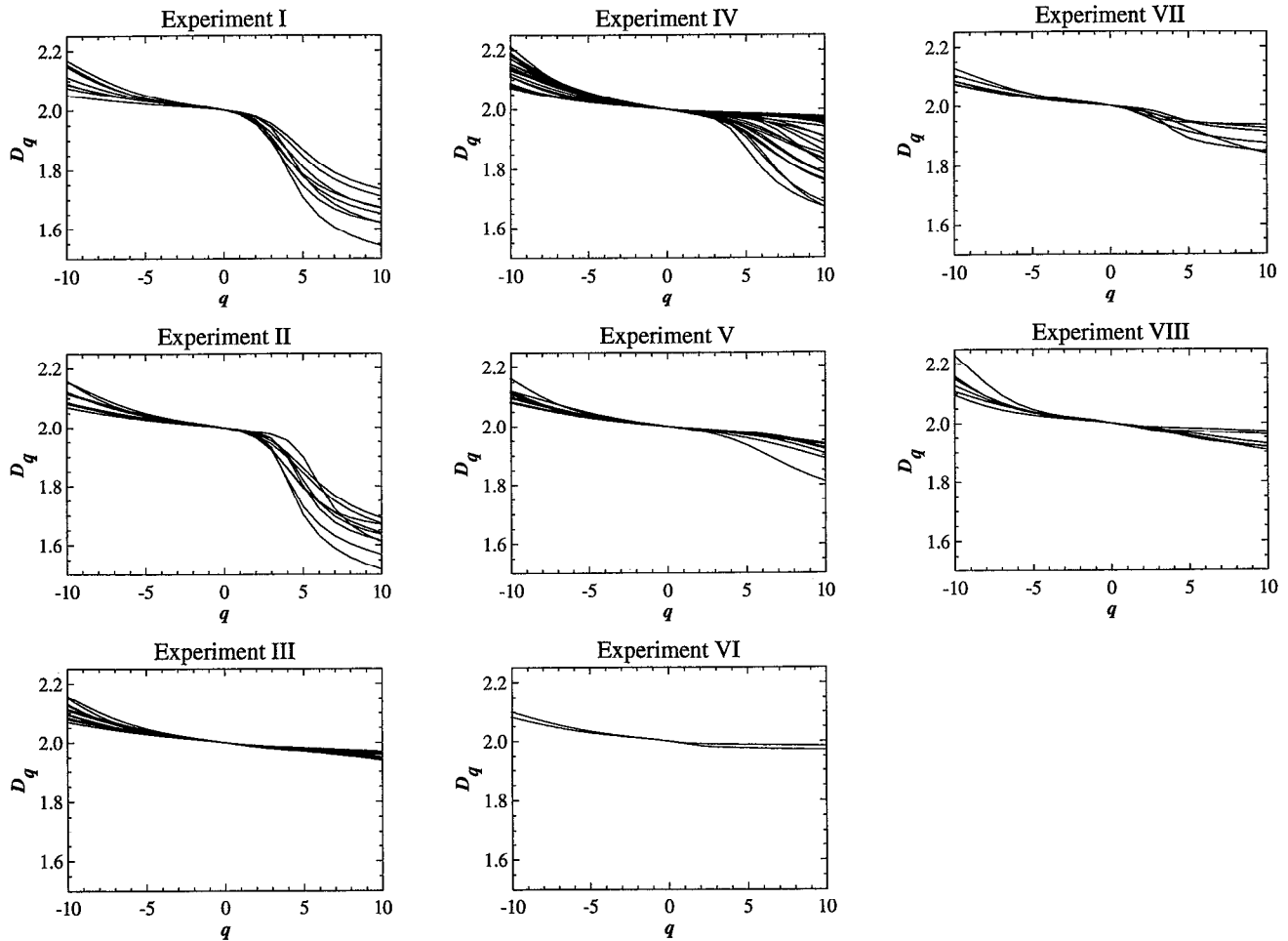


Figure 6. Generalized dimensions D_q versus moments q for DNAPL experiments.

terns of these plots identify the spatial distribution of the DNAPL and are also interpretable as relative DNAPL saturation.

Almost identical patterns were attained for the repetitions of the same experiment with different initial and boundary conditions (experiments V-a through V-c). We conjecture that a particular combination of sand and DNAPL yields a specific fractal pattern, independent of the spill conditions.

In Figure 5 we present results of this analysis for all experiments. The pattern of experiment V-a is herein taken as representative for experiments V. It was found for experiments I and IV that both systems with TCE are characterized by a wide intensity range at the infiltration front and approximately a straight decline in the fractal distribution versus relative intensity (symbolized as a back slash). Dibutyl phthalate (DBP) likewise revealed a wide range for the penetration front in experiments III and VI, but has a concave fractal spectrum (\cap). For experiments II and V with TCA, we recognize a small range at the front and a maximum intensity at half the depth of penetration. The fractal spectrum here is typically concave-convex ($\cap\cup$). Contrasting such correlation of patterns from coarse to medium sand for all tested DNAPLs, a similarity subsists among the patterns developed in fine sand (experiments VII and VIII). The highest intensities are depicted in the top portion of the plumes, and the fractal distribution is generally concave (\cap or $\cap\cap$). None of the characteristics seen

in the coarser two sands are evident for displacement by TCE and TCA in the fine sand.

This leads us to the interpretation that the porous medium defines the pattern for the DNAPLs in fine sand, whereas the DNAPL properties determine the distribution pattern in very coarse and medium sand. According to these findings a clear distinction between displacement regimes is suggested: viscous fingering in the coarser porous media and capillary fingering in the fine porous media (compare to the phase diagram, Figure 1).

3.2. Multifractal Analysis

Plots of $\log \chi_q(\varepsilon)$ versus $\log \varepsilon$ gave a good linear fit for $\tau(q)$, which justifies the application of the method of moments [Evertsz and Mandelbrot, 1992, p. 942]. Hence the method of moments should produce the correct results. Complete diagrams of D_q and $f(\alpha)$ functions for the experiments are presented in Figures 6 and 7. We did not plot error estimates, since all cross sections of an experiment are overlotted in one graph and give an idea of the spread in the data.

The generalized dimensions D_q offer an interpretation of the measure with respect to modeling approaches. Måløy *et al.* [1987] observed a quantitative change in the scaling exponents D_q between fingering in diffusion-limited aggregation (DLA) and invasion percolation models. The slope of D_q for positive q is taken as an indication of the degree of self-similarity of the structure. D_q should be constant for an exactly self-similar

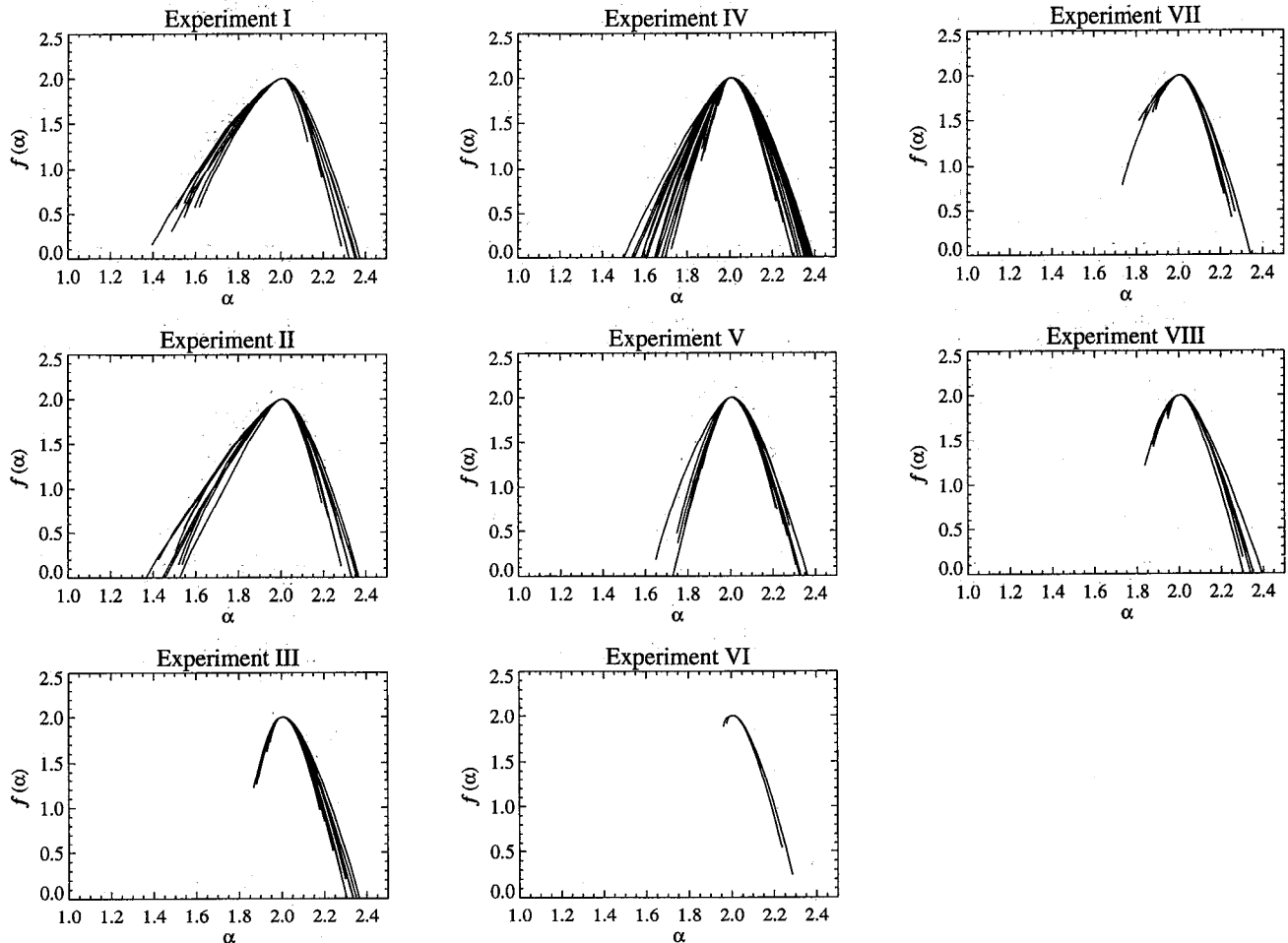


Figure 7. Spectrum of singularities $f(\alpha)$ versus singularity strength α for DNAPL experiments.

cluster. A flat slope of the curve is expected for the compact structures in the invasion percolation regime. Experiments III, VI, VII, and VIII in Figure 6 would then confirm an invasion percolation type structure. A crossover to DLA type structures with steeper gradients is perceived in experiments I and II.

The $f(\alpha)$ functions in Figure 7 were computed directly [after Chhabra and Jensen, 1989]. The $f(\alpha)$ from the sections of a specific experiment are found to be stable. All $f(\alpha)$ spectra are nontrivial, with a fairly large range of α . A consistent widening of the left part of the curves, for the range of $\alpha_{q=0}$ to $\alpha_{q=+10}$, is seen in our experiments from fine to coarse sands and from DBP to TCE. The ranges of α for positive moments increase from 0.05 (in experiment VI) to 0.6 (in experiment I). The α ranges for the negative moments are unchanged. It is recognized that the error margins grow with larger moments. The error estimates for positive moments were such that the widening of $f(\alpha)$ is confirmed in the above limits.

According to Lutsko *et al.* [1992], the broadening of the $f(\alpha)$ spectrum indicates destabilizing factors in the displacement. They documented numerically a widening of the α spectrum by lowered surface tensions or enlarged porosities. We showed that a higher density contrast and higher viscosity contrast have the same effect and can be added to that list. These findings are in agreement with the theory of displacement stability [see Chuoke *et al.*, 1959]. The $f(\alpha)$ functions are fully quantitative and allow a consistent classification of DNAPL displacement in porous media.

The extreme values of the coarse Hölder exponent, α_{\min} and α_{\max} , usually converge to $f(\alpha) = 0$; α_{\min} and α_{\max} correspond to the moments $q \rightarrow +\infty$ and $q \rightarrow -\infty$, respectively. The fact that the spectrum $q \rightarrow +\infty$ ends at a finite $f(\alpha)$ value is assigned to a phase transition or given a physical interpretation: The densest parts of the measure are not contracted to points, but fill up some space [Halsey *et al.*, 1986]. The finite values of $f(\alpha)$ relate to a high fractal dimension at large positive moments or the flat slope in D_q . Such behavior of $f(\alpha)$ is seen in Figure 7 for the experiments with a more stable displacement configuration. In the sections of experiment IV we did observe a transition from an upper stable plume to dominant fingering, which is revealed in $f(\alpha_{q=+10})$ as a shift from nonzero values to zero.

4. Discussion

With a statistical object analysis, phenomenological characteristics of the DNAPL distributions were measured that had been observed during disassembly of the experiments. Criteria to classify all experiments could not be found by investigating areas, perimeters, or intensities in the usual sense. The fractal nature of the DNAPL distribution was implied from our images and led us to a scaling analysis.

Fingering in fluid-fluid displacement does not necessarily produce fractal geometries. An attraction to nonfractal regimes for viscosity-controlled displacements is suggested by

Lee et al. [1990]. The randomness of the process is assumed as decisive for fractality of the displacement structures [Chen, 1987]. We demonstrated that fractal fingers are created under experimental conditions with real porous media. Irregularities and randomness exist in the pore network at small length scales and give rise to complex process dynamics.

The literature reports a lower scale cutoff in immiscible displacement. The effects of wetting properties and interface velocity at the pore scale have been discussed in that context [Weitz et al., 1987; Cieplak and Robbins, 1988]. The same mechanisms probably opposed a fractal scaling of the perimeter at high resolutions. Fractal behavior is expected to extend only down to the pore scale; for the coarse sand our image resolution actually exceeded the mean pore size. A lower limit for geometrical scaling can be physically foreseen. An upper limit of scaling was imposed experimentally with the limited size of the spill.

The fractal patterns of the DNAPL distributions (Figure 6) can be looked at as a fingerprint of the respective displacement system. For each system of DNAPL and porous medium we found a probabilistic scaling behavior that indicates the fingering regime, dominated either by viscous and gravitational forces or by capillarity. These patterns describe the spatial distribution or variation of relative DNAPL saturations resulting from a spill situation.

Employment of multifractal formalisms on our data was motivated by the idea of retrieving dynamical information of the system from multifractal scaling properties [see Jensen, 1987]. This would be possible if the underlying dynamical processes are well defined. Such information may not be retrievable for the kind of data we have. We restrict ourselves in this study to presenting multifractal spectra of the experiments for the quantification and classification of displacement instability.

Several formalisms for the determination of multifractal behavior have been employed in our study, for example, those according to Vicsek [1990] and Lutsko et al. [1992] (based on a correlation integral), or Halsey et al. [1986] and Chhabra and Jensen [1989] (based on box counting). The calculation of negative moments from experimental data was found particularly difficult and brought about obscure results for the former of the above procedures. It should be noted that good convergence of negative moments is rarely found, even for mathematical constructions of a multifractal.

When we used the images as a whole, including intensity values of the background and the DNAPL range, the methods based on box counting produced straight-line fits for positive and negative moments and a continuous $f(\alpha)$ curve. There was no procedure for eliminating all the background information in the images that would not lead to the loss of scaling behavior for negative moments. The range of negative moments was thus affected by image information of the background. We try to avoid the term noise in this context, since these readings reflect the structure of the porous medium. They may have a greater influence on the displacement dynamics and on the resulting DNAPL distributions than one might perceive at first.

The positive moments of the D_q function and corresponding left-hand side of the $f(\alpha)$ function, however, can be clearly attributed to the DNAPL distribution. D_q relates structures to a type of fingering simulated with probabilistic models [Måløy et al., 1987]. The spectrum of singularities $f(\alpha)$ is remarkably stable for all sections of an experiment. They show a consistent widening of the α range from fine to coarser sands and from highly viscous to less viscous DNAPL. In other words, the

range of α is related to the stability in the DNAPL displacement. Destabilizing factors are seen in a coarser pore network, higher density, and lower viscosity of the DNAPL. We computed finite values of $f(\alpha)$ for large positive moments in several experiments. They ordinarily indicate a phase transition in the dynamical system.

We also tested higher-order correlation functions, i.e., lacunarity, as a descriptor for the displacement systems. The scaling averages in a fractal and multifractal approach lump some information together that is valuable for a refined analysis of the physical mechanisms and dynamics. Multifractality still seems to be a suitable approach for the quantification of hydrodynamic instabilities in porous media. A theoretical or numerical model of DNAPL fingering should match the documented multifractal behavior as a necessary condition.

The combination of the above analyses allows the characterization and classification of DNAPL fingering in porous media. The system configurations, the combinations of sand and DNAPL, cover fingering phenomena from a dominantly gravitational regime to viscous and capillary fingering, and rather stable displacements.

Acknowledgments. We thankfully acknowledge Mogens Jensen and Tom Over for their input and assistance. Financial support was provided by the U.S. EPA through the Hazardous Substances Research Center at Kansas State University. The first author gratefully acknowledges a scholarship granted by the Rotary Foundation.

References

- Chandler, R., J. Koplik, K. Lerman, and J. F. Willemsen, Capillary displacement and percolation in porous media, *J. Fluid Mech.*, 119, 249–267, 1982.
- Chen, J. D., Pore-scale difference between miscible and immiscible viscous fingering in porous media, *AIChE J.*, 33(2), 307–311, 1987.
- Chhabra, A., and R. V. Jensen, Direct determination of the $f(\alpha)$ singularity spectrum, *Phys. Rev. Lett.*, 62(12), 1327–1330, 1989.
- Chuoke, R. L., P. van Meurs, and C. van der Poel, The instability of slow, immiscible, viscous liquid-liquid displacements in permeable media, *Trans. Am. Inst. Min. Metall. Pet. Eng.*, 216, 188–194, 1959.
- Cieplak, M., and M. O. Robbins, Dynamical transition in quasistatic fluid invasion in porous media, *Phys. Rev. Lett.*, 60(20), 2042–2045, 1988.
- Clément, E., C. Baudet, and J. P. Hulin, Multiple scale structure of nonwetting fluid invasion in 3D model porous media, *J. Phys. Lett.*, 46, L1163–L1171, 1985.
- Daccord, G., J. Nittmann, and H. E. Stanley, Radial viscous fingers and diffusion-limited aggregation: Fractal dimension and growth sites, *Phys. Rev. Lett.*, 56(4), 336–339, 1986.
- Evertsz, C. J. G., and B. B. Mandelbrot, Multifractal measures, in *Chaos and Fractals*, edited by H.-O. Peitgen, H. Jürgens, and D. Saupe, pp. 921–953, Springer-Verlag, New York, 1992.
- Feder, J., *Fractals*, Plenum, New York, 1988.
- Frisch, U., and G. Parisi, Fully developed turbulence and intermittency, in *Turbulence and Predictability of Geophysical Flows and Climate Dynamics*, edited by M. Ghil, R. Benzi, and G. Parisi, pp. 85–86, North-Holland, New York, 1985.
- Gee, G. W., C. T. Kincaid, R. J. Lenard, and C. S. Simmons, Recent studies of flow and transport in the vadose zone, in *U.S. Natl. Rep. Int. Union Geod. Geophys. 1987–1990, Rev. Geophys.*, 29, 227–239, 1991.
- Glass, R. J., S. Cann, J. King, N. Baily, J.-Y. Parlange, and T. S. Steenhuis, Wetting front instability in unsaturated porous media: A three-dimensional study in initially dry sand, *Transp. Porous Media*, 5, 247–268, 1990.
- Halsey, T. C., M. H. Jensen, L. P. Kadanoff, I. Procaccia, and B. I. Shraiman, Fractal measures and their singularities: The characterization of strange sets, *Phys. Rev. A*, 3, 1141–1151, 1986.
- Held, R. J., and T. H. Illangasekare, Fingering of dense nonaqueous

- phase liquids in porous media, 1, Experimental investigation, *Water Resour. Res.*, this issue.
- Hentschel, H. G. E., and I. Procaccia, The infinite number of generalized dimensions of fractals and strange attractors, *Physica D*, 8, 435–444, 1983.
- Homsy, G. M., Viscous fingering in porous media, *Annu. Rev. Fluid Mech.*, 19, 271–311, 1987.
- Jensen, M. H., Multifractals: Formalism and experiments, in *Time-Dependent Effects in Disordered Materials*, edited by R. Pynn and T. Riste, pp. 173–183, Plenum, New York, 1987.
- Lee, J., A. Coniglio, and H. E. Stanley, Fractal-to-nonfractal crossover for viscous fingers, *Phys. Rev. A*, 41, 4589–4592, 1990.
- Lenormand, R., Différents mécanismes de déplacements visqueux et capillaires en milieux poreux: Diagramme de phase, *C. R. Acad. Sci., Ser. 2*, 310, 247–250, 1985.
- Lutsko, J. F., J. P. Boon, and J. A. Somers, Lattice gas automata simulations of viscous fingering in a porous medium, in *Numerical Methods for the Simulation of Multi-phase and Complex Flow, Proceedings, Amsterdam, 1990*, edited by T. M. M. Verheggen, pp. 124–135, Springer-Verlag, New York, 1992.
- Måløy, K. J., J. Feder, and T. Jøssang, Viscous fingering fractals in porous media, *Phys. Rev. Lett.*, 55(24), 2688–2691, 1985.
- Måløy, K. J., F. Boger, J. Feder, and T. Jøssang, Dynamics and structure of viscous fingering in porous media, in *Time-Dependent Effects in Disordered Materials*, edited by R. Pynn and T. Riste, pp. 111–138, Plenum, New York, 1987.
- Mandelbrot, B. B., *The Fractal Geometry of Nature*, W. H. Freeman, New York, 1982.
- Mandelbrot, B. B., Multifractal measures, especially for the geophysicist, *Pure Appl. Geophys.*, 131, 5–42, 1989.
- Meakin, P., Fractal aggregates in geophysics, *Rev. Geophys.*, 29(3), 317–354, 1991.
- Nittmann, J., G. Daccord, and H. E. Stanley, Fractal growth of viscous fingers: Quantitative characterization of a fluid instability phenomenon, *Nature*, 314, 141–144, 1985.
- Nittmann, J., H. E. Stanley, E. Touboul, and G. Daccord, Experimental evidence of multifractality, *Phys. Rev. Lett.*, 58(6), 619, 1987.
- Oxaal, U., M. Murat, F. Boger, A. Aharony, J. Feder, and T. Jøssang, Viscous fingering in percolation clusters, *Nature*, 329, 32–37, 1987.
- Paterson, L., Diffusion-limited aggregation and two-fluid displacements in porous medium, *Phys. Rev. Lett.*, 52(18), 1621–1624, 1984.
- Peters, E. J., and D. L. Flock, The onset of instability during two-phase immiscible displacement in porous media, *SPEJ Soc. Pet. Eng. J.*, 21, 249–258, 1981.
- Vicsek, T., Mass multifractals, *Physica A*, 168, 490–497, 1990.
- Weitz, D. A., J. P. Stokes, R. C. Ball, and A. P. Kushnick, Dynamic capillary pressure in porous media: Origin of viscous-fingering length scale, *Phys. Rev. Lett.*, 59(26), 2967–2970, 1987.
- Wilkinson, D., and J. F. Willemsen, Invasion percolation: A new form of percolation theory, *J. Phys. A*, 16, 3365–3376, 1983.
- Wooding, R. A., and H. J. Morel-Seytoux, Multiphase fluid flow through porous media, *Annu. Rev. Fluid Mech.*, 8, 233–274, 1976.
- Yortsos, Y. C., Instabilities in displacement in porous media, *J. Phys. Condens. Matter*, 2, SA443–SA448, 1990.

R. J. Held and T. H. Illangasekare, Department of Civil, Environmental, and Architectural Engineering, University of Colorado, Boulder, CO 80309. (e-mail: illangas@gwater.colorado.edu)

(Received April 28, 1994; revised January 17, 1995; accepted February 2, 1995.)